Analysis of calibration differences between MODIS and MISR

A. Lyapustin[a], Y. Wang[a], R. Kahn[b], J. Xiong[c], A. Ignatov[d], R. Wolfe[c],
A. Wu[e], C. Bruegge[b]

[a]University of Maryland, Baltimore County, Baltimore, MD 21250, and NASA Goddard Space Flight Center, mail code 614.4, Greenbelt, MD 20771
[b]NASA Jet Propulsion Laboratory, Pasadena, CA 91109
[c]NASA Goddard Space Flight Center, Greenbelt, MD 20771
[d]NOAA/NESDIS, Camp Springs, MD 20746
[e]Science Systems and Applications, Inc., Lanham, MD 20706.

ABSTRACT

MODIS and MISR are two Earth Observing System instruments flown onboard Terra satellite. Their synergistic use could greatly benefit the broad user community by ensuring the global view of the Earth with high-quality products. A necessary condition for data fusion is radiometric calibration agreement between the two instruments. Earlier studies showed about 3% absolute radiometric difference between MISR and respective MODIS land bands in the visible and near-IR spectrum, which are also used in aerosol and cloud research. This study found a systematic bias of +(0.01-0.03) between two surface albedo products derived from MODIS and MISR L1B data using the AERONET-based Surface Reflectance Validation Network (ASRVN). The primary cause of the bias is inconsistencies in the cross-sensor calibration. To characterize MODIS-MISR calibration difference, top-of-atmosphere MODIS and MISR reflectances were regressed against each other over liquid water clouds. The empirical regression results have been adjusted for the differences in the respective MISR and MODIS spectral responses using radiative transfer simulations. The MISR-MODIS band gain differences estimated with this technique are +6.0% in the blue, +3.3% in the green, +2.7% in the red, and +0.8% in the NIR band. About 2.1%-3.6% of the difference in the blue band is due to the difference in the MODIS-MISR solar irradiance models.

Keywords: MODIS, MISR, cross-calibration, cloud reflectance, spectral correction

1. INTRODUCTION

MODIS and MISR are two major Earth Observing System (EOS) [1] instruments flown onboard of TERRA satellite, and used to produce global information about aerosol, cloud and land surface parameters. An optimal synergy of MODIS-MISR products could greatly benefit the broad user community.

At present, the MODIS and MISR absolute radiometric scales are known to differ by about 3% over most of the visible spectrum [2-4]. This difference propagates into the higher level land, ocean and atmospheric products, impeding the data fusion applications and science data analysis. We found this difference in the surface albedo derived by the AERONET-based Surface Reflectance Validation Network (ASRVN). The ASRVN [*in preparation*] is an operational processing system that receives MODIS and MISR calibrated reflectance (L1B) data around 160 AERosol RObotic NETwork (AERONET) [5] sites globally, and uses AERONET well-calibrated aerosol and water vapor data to independently and self-consistently derive surface bi-directional reflectance factor (BRF) and albedo. The ASRVN retrievals show a systematic positive MISR-MODIS albedo bias of +(0.01-0.03). Because spectral band differences are accounted for through the radiative transfer, the most likely explanation for the bias is a calibration inconsistency between the sensors.

The two instruments employ different calibration strategies, and known radiometric differences of about 3% are within the uncertainties of the respective calibration methods. A brief overview of the MODIS and MISR calibration procedures and associated accuracies is given in Section 2.

To independently assess the MISR-MODIS calibration differences, we regressed MISR-MODIS TOA reflectances over liquid water clouds, with a theoretical correction for the sensors spectral differences. The methodology and results of the

Remote Sensing and Modeling of Ecosystems for Sustainability III, edited by Wei Gao, Susan L. Ustin,
Proc. of SPIE Vol. 6298, 62980X, (2006) · 0277-786X/06/$15 · doi: 10.1117/12.680896

regression analysis are described in section 3. This section also investigates the effect of different solar irradiance models used in MODIS and MISR calibration that can explain about a half of the observed band gain difference in the blue band. Section 4 summarizes and concludes this study.

2. OVERVIEW OF MODIS AND MISR CALIBRATION IN THE REFLECTIVE SOLAR BANDS

The two sensors employ different calibration strategies: MODIS uses onboard calibration devices whereas MISR relies on a combination of vicarious calibration experiments and onboard band-to-band and camera-to-camera relative calibration tests, to establish its absolute radiometric scale. Both MODIS and MISR teams have been conducting comprehensive calibration and characterization instrument analyses [2-3, 6-16]. The two instruments have shown a good agreement for lunar observations taken early on in the TERRA satellite mission [3]. The systematic discrepancy in absolute radiance was found later in the vicarious experiments over both bright desert targets [15] and ocean, in low light conditions [16].

2.1 MODIS

MODIS makes observations in 20 reflective solar bands (RSB) at three nadir spatial resolutions (250m for bands 1-2, 500m for bands 3-7, and 1km for bands 8-20) over a wide field-of-regard ($\pm 55^{o}$). MODIS L1B geolocated and radiometrically calibrated data products include TOA reflectance factors and spectral radiances. In order to monitor and maintain on-orbit calibration accuracy and data product quality, the instrument was designed with a set of on-board calibrators, including a solar diffuser (SD) and a solar diffuser stability monitor (SDSM) system for the RSB calibration, and a spectro-radiometric calibration assembly for the sensor's spectral and spatial characterization [6-9, 2, 11]. The calibration accuracy requirements (1σ at the typical scene radiances) are ±2% for the RSB reflectance factors and ±5% for the radiance product. MODIS RSB calibration uses look-up tables derived from SD/SDSM measurements. On-orbit, the SD/SDSM system is operated on a bi-weekly basis to track the RSB response changes.

MODIS SD panel is made of space grade Spectralon material, with a near-Lambertian reflectance profile in the RSB spectral range. Its bi-directional reflectance factor (BRF) was carefully characterized pre-launch by the instrument vendor (Raytheon/Santa Barbara Remote Sensing) using a comparison approach with reference samples traceable to the reflectance standards of the National Institute of Standards and Technology. The BRF profiles for some reflective solar bands were also validated on-orbit using data collected during spacecraft maneuvers [10]. Solar exposure of the SD panel causes the SD BRF to degrade. The rate of SD BRF changes is wavelength dependent. For this reason, the SDSM is operated during each scheduled SD calibration event. The SDSM, which has its own spectrally-filtered detectors, works as a ratioing radiometer. It tracks the SD BRF on-orbit degradation using its simultaneous responses to the direct sunlight and that diffusely reflected from the SD panel [9]. For Terra MODIS, the response changes have been approximately 2% at 0.47μm (band 3) and less than 1% at 0.86μm (band 2) per year over its nearly 6 years of on-orbit operation.

2.2 MISR

Data from both vicarious calibration experiments and the on-board calibration system play key roles in the MISR radiometric calibration process [3, 13]. Vicarious field data provide input to a radiative transfer code that simulates MISR band-weighted top-of-atmosphere radiances. The MISR calibration process is adjusted so the Level 1B2 Geolocated Radiance Product values equal those measured during the 2000 field campaign at Railroad Valley. Subsequent vicarious calibration experiments have served to verify the accuracy of the radiance data product. Annual field measurements are made at homogeneous desert playa sites such as Lunar Lake, Railroad Valley, Ivanpah, and Black Rock Desert, all in Nevada, under clear sky and low aerosol conditions, to verify the results and help monitor calibration changes. The precision of the vicarious absolute calibration is estimated to be 2-4% ($1\ \sigma$), and is best for the MISR Green and Red bands, whereas the band-to-band and camera-to-camera uncertainties appear to be in the 1-2% range [3].

MISR response degradation has been approximately 2% per year over the first five years in flight. To account for drifts from the 2000 scale determination, the MISR team makes use of an on-board calibrator. Here bi-monthly observations are made of sunlight reflected by diffuse-reflecting, Lambertian standards. These panels are made of pristine Spectralon, and have not degraded during the first five years of the mission [e.g., 14]. On-board photodiode detectors measure the panel-reflected radiances. Diode field-of-view and solar spectrum differences are taken into account as part of the

calibration analysis, and the panels themselves are assumed white, based on pre-launch studies. The individual cameras and secondary diodes then view the sun-lit panels simultaneously to complete the camera-to-camera on-board calibration. Since the cameras do not all view the panels at the same angle as the calibration diodes, panel bi-directional reflectance functions are used. These were also measured pre-launch, and are checked periodically by another on-board diode package mounted on a goniometer. The detectors were initially calibrated using the 2000 vicarious calibration campaign observations. Degradation of the photodiodes is accounted for by response adjustments against a specific photodiode, the Blue High-Quantum-Efficiency diode, which has been stable throughout the mission to date [14].

To further validate the band-to-band and camera-to-camera radiance scales, the MISR Team analyzed a set of observations taken when the Terra spacecraft was rotated to observe the moon, multiple observations over uniform, dark water having identical geometry relative to the solar equator, and radiance comparisons with MODIS [3; 15]. The low-light-level calibration was tested further by assessing MISR radiances relative to a radiative transfer model constrained by AERONET observations taken around deep ocean island sites [16]. To first order, MISR reported absolute radiances are 3% higher than MODIS, when compared over homogenous scenes. This has been traced to differences between the vicarious calibration scale adopted for MISR, and the on-board standard used for MODIS.

3. MISR-MODIS CROSS-CALIBRATION OVER CLOUDS

The optically thick water clouds are spectrally flat in the visible and NIR region and thus can serve as a calibration transfer standard as described in section 3.1. This approach has been used to cross-calibrate the AVHRR sensors [17-18].

The interpretation of the empirical regression slopes in terms of the sensors calibration gain ratios is not straightforward because of the spectral differences between the MISR and MODIS bands (Figure 1). To quantify this effect and derive sensors gain ratio, radiative transfer model (RTM) simulations were performed (section 3.2), and the empirical regression results were then adjusted for the MISR-MODIS spectral differences.

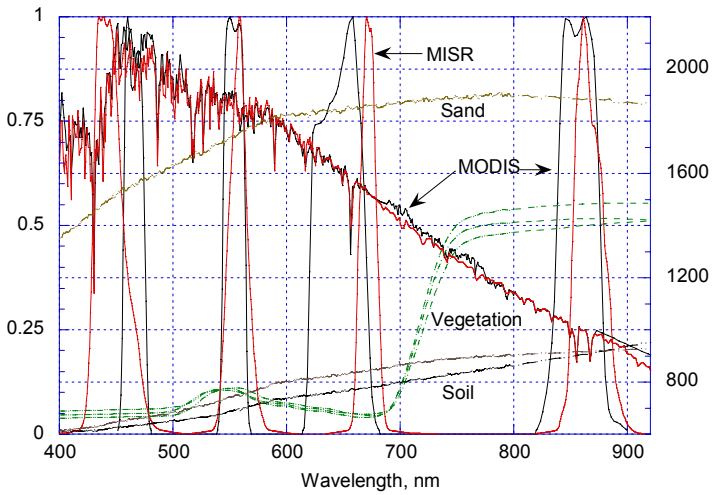

Figure 1. Relative spectral response functions of MISR (red) and MODIS land channels (black). Also shown are models of MODIS and MISR spectral solar irradiance ($Wm^{-2}\mu m^{-1}$), and reflectance spectra of several types of soil, sand, and vegetation.

3.1. Empirical results

For this work, the ASRVN was augmented to include a separate processing of MISR TOA reflectances from the nadir camera (An, VZA<15^o) and corresponding MODIS near-nadir reflectances. MODIS and MISR data are first re-projected and then averaged over an area of 32×32 km^2 to minimize the effect of different projections and pixel sizes. The experimental regressions are shown in Figure 2, top row. These data represent most of the AERONET stations on different continents, covering different seasons, and the full range of solar zenith angles. Figure 2 has N=1,500 data points accumulated between November 2005 and February 2006.

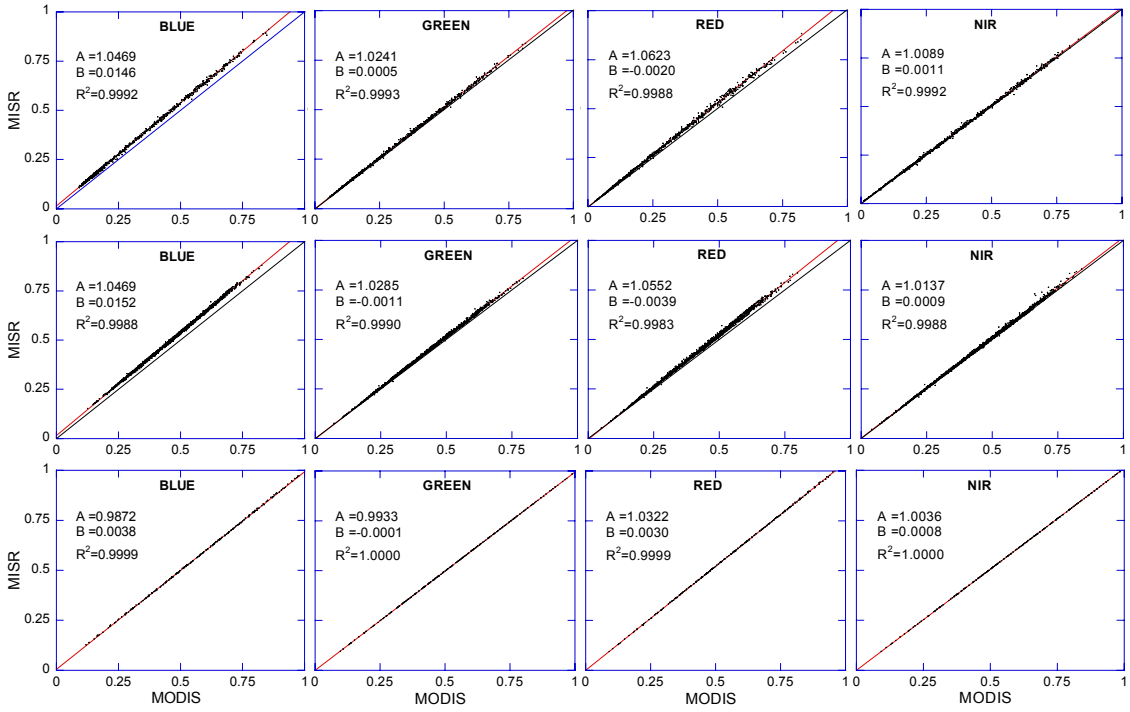

Figure 2. Experimental and theoretical regressions of MODIS-MISR TOA L1B reflectance over clouds. The plots of top and middle rows represent data collected over the land and over the ocean. The bottom row shows theoretically calculated regression lines.

The regression only contains points for which the ASRVN cloud mask algorithm detected at least 50% cloudy pixels inside the averaging box (32×32 km^2). With this definition, regression points may include a mixture of clear pixels, and continuous or broken clouds of different optical depths, which can be both liquid water and ice. We have tested the sensitivity of the empirical regression to the 50% threshold varying it from 40% to 70% and found that it has very little effect on the regression parameters. For example, adding non-cloudy pixels in the averaging box only slightly increases scatter around the low end of regression in the visible bands and practically has no effect on its slope and offset. The effect of scatter is larger in the NIR band, but still the effect on the regression parameters was minimal. By trial and error, the 50% threshold was found to be adequate.

As a sensitivity check, and for better agreement with our theoretical analysis (see sec. 3.2), an independent set of MODIS and MISR L1B data was collected over the ocean in pristine maritime conditions: off the southern coast of Peru, coasts of California, Namibia and Zimbabwe, and off the east coast of Asia, 44 MODIS and corresponding MISR granules in total. The MODIS Cloud Phase (MOD06) product was used to select points representing liquid water clouds. The view geometry was restricted to the non-glint conditions defined as R_{CM}<0.02, where R_{CM} is a calculated Cox-Munk [19] reflectance of the roughened water surface at the wind speed of 10 m/s. This restriction helped us to eliminate a few remaining outliers in the data. The regressions for N=1,600 points collected in January – February 2006 are shown in Figure 2, middle row.

Interestingly, the results for the carefully screened oceanic water clouds are very close to the mixed-case results obtained over land. This may indicate that ice clouds can also be used as targets for the cross-calibration analysis using this method. The regression results over the land and over the ocean are practically identical in the Blue band. In the other three bands, the differences in the slopes and intercepts are larger, but they are still statistically insignificant (i.e. less than uncertainties of the regression coefficients).

The regressions obtained represent different regions of both the Northern and Southern hemispheres. The regression lines were found to stabilize after about N=500 data points have been accumulated. Nevertheless, larger and more

representative statistics continue to be collected, to investigate possible regional and seasonal variability in experimental regressions.

The empirical regression coefficients MISR=A×MODIS+B from Figure 2 are summarized in Table 1. Here, the "Measured" row lists the average coefficients between the land and the ocean. Except for the Blue band, the offset of the regression is within the regression error and should be set to zero. This is expected because the radiometric offsets in both MISR and MODIS reflectance are specified from space counts and are therefore known very accurately. The reason for the offset anomaly in the Blue band is unknown. The average empirical slopes are 1.047, 1.026, 1.059 and 1.011 for the Blue, Green, Red and NIR bands, respectively.

	A_B	B_B	A_G	B_G	A_R	B_R	A_{NIR}	B_{NIR}
1. Measured	1.047	0.015	1.026	-0.003	1.059	-0.003	1.011	0.001
2. Simulated	0.987	0.004	0.993	-0.000	1.032	0.003	1.003	0.001
3. Difference	0.060	0.011	0.033	-0.003	0.027	-0.006	0.008	0.000

Table 1. Summary of slope and offset regression coefficients. The "Measured" coefficients represent the average between the land and the ocean. The numbers have been rounded to third significant digit.

3.2. Simulations

Reflectance of water clouds have been simulated using Mie theory and a narrow-band radiative transfer code that can account for the difference in the relative spectral responses (RSR) of the sensors analyzed. The simulated spectral TOA radiance is expressed as:

$$L_{\Delta\lambda} = \int \frac{F_\lambda}{\pi} I_\lambda h_\lambda d\lambda \Big/ \int h_\lambda d\lambda \,, \tag{1}$$

where F_λ is the extraterrestrial spectral solar irradiance, I_λ is monochromatic TOA radiance calculated for F_λ=π, h_λ is RSR of sensor. The TOA radiance and reflectance (R) are related via the band-dependent solar irradiance ($E_{\Delta\lambda}$),

$$L_{\Delta\lambda} = RE_{\Delta\lambda}/\pi \,,\; E_{\Delta\lambda} = \int F_\lambda h_\lambda d\lambda \Big/ \int h_\lambda d\lambda \,. \tag{2}$$

The standard MODIS L1B reflectance product is corrected for out-of-band spectral contributions, whereas the MISR L1B reflectance is not (this correction is made later during L2 processing). To take this difference into account, the spectral limits of integration were selected to represent the in-band spectral intervals for MODIS, and the total spectral interval where RSR is defined (365 – 1100 nm) for MISR [20].

The radiative transfer calculations in this work were done with SHARM code [21] and the Interpolation and Profile Correction (IPC) method [22]. The IPC method is designed for fast line-by-line calculations in the spectral interval of interest with flexible spectral resolution of 0.01 – 1 cm^{-1} and an accuracy of several tenths of a percent. The line-by-line calculations are then integrated directly with solar irradiance and sensor' band-pass functions. The absorption of 7 major atmospheric gases (H_2O, CO_2, O_3, CH_4, NO_2, CO, N_2O) was included based on the HITRAN-2000 [23] database and the Atmospheric Environmental Research continuum absorption model [24], with a Voigt vertical profile. For radiative transfer in clouds, the SHARM code uses the Delta-M method.

The radiative transfer calculations were done with constant cloud top height (2 km) and column water vapor (1.5 cm) with the US 1976 Standard Atmosphere profile. The water clouds were modeled using a log-normal size distribution with mean radius r_g =6, 10, 15, 20 μm, and standard deviation σ_g=0.1, 0.35, scalable cloud optical depth τ_c=3.7 – 130, and optical spectral properties of water from *Hale and Querry* [25]. The mean radius for the log-normal distribution is close to the effective radius, typically used in cloud research and defined as a ratio of the third and the second moments of the size distribution. For example, for the simulated cases with σ_g=0.1, 0.35, the ratio of radii is r_g/r_{eff}=1.025, 1.28, respectively.

A sensitivity study of theoretical regression coefficients shows that natural variability of cloud droplet size, cloud top height, and atmospheric moisture play relatively minor roles, causing a factor of 4-10 smaller variation than the band

gain differences studied (sec. 3.3). The calculated theoretical regressions are shown in the bottom row of Figure 2. They are linear in the full dynamic range of the signal with non-linearity less than 0.5%, and have very little scatter. The theoretical slopes are 0.987, 0.993, 1.032, and 1.004 in the Blue, Green, Red and NIR bands, respectively.

3.3 Sensitivity of theoretical regression to atmospheric variability

Extensive simulations were conducted for the near-nadir view geometry (VZA<15^o) and a wide range of solar zenith angles ($0^o \le SZA \le 75^o$) studying the effect of cloud droplet size distribution, water vapor and cloud top height variations on the regression coefficients. Simulations revealed the following results:

- The effect of solar zenith angle is small in the Blue and Red bands, and it is negligible in the Green and NIR. On the other hand, the regression is slightly non-linear. For instance, increase of SZA range to 0^o-75° from the range 0^o-51° changes slope of regression from 0.989 to 987 in the Blue, and from 1.029 to 1.032 in the Red.

- Table 2 shows dependence of the regression coefficients on the effective size of water droplets. Blue and Red bands, in which the band-pass functions between MODIS and MISR differ most, were chosen for this sensitivity check. With the modal droplet radius changing from 6 to 20 μm, the slope of the regression changes from 0.993 to 0.978 in the Blue, and from 1.029 to 1.037 in the Red bands. The category "All" gives the average coefficients for the cumulative regression, which might be a little skewed towards clouds having the smallest effective radii. This happens because small droplets produce the highest optical depth in Mie calculations at the same droplet concen tration. In turn, this gives the points with highest radiance, which may offset the total regression somewhat. In the future, we may weight our calculations for different radii with realistic regional cloud droplet size probability distribution functions, derived, for example, from the MODIS cloud product (MOD06).

r_g, μm	6	10	15	20	All
A_B	0.991	0.986	0.980	0.976	0.987
A_R	1.029	1.035	1.036	1.037	1.032

Table 2. Dependence of slope in the Blue and Red bands on the effective droplet size. Simulations were done for 1976 US Standard Atmospheric Profile, with the column atmospheric water vapor column of 1.5 cm and cloud top height of 2 km.

- Table 3 shows that the regression slope in the Blue band is only weakly sensitive to the cloud top height. This sensitivity is due to the Rayleigh scattering above the cloud. In the Red band, this effect is a about a factor of 2.5 smaller and is probably caused by the re-distribution of water vapor absorption above the cloud. There is practically no dependence in the spectrally close Green and NIR bands.

	H_c (1-5km)	CWV (0.4-2.0-5.0 cm)
A_B	0.984-0.991	-
A_G	-	-
A_R	1.034-1.037	1.033-1.037-1.052
A_{NIR}	-	1.002-1.008-1.017

Table 3. Effect of cloud top height (H_c) and column water vapor (CWV) on the slope of regression, calculated for r_g=10 μm. The dependence on the cloud top height was calculated for CWV=0.5 cm. The dependence on the CWV was evaluated for H_c =2 km.

- The regression slope for the Red and NIR bands has a rather weak dependence on the column water vapor (Table 3), as long as the high moisture conditions (≈3.5-5 cm), typical of tropical geographical belt, are avoided.

Thus, simulations show that sensitivity of this method to the natural atmospheric variability is relatively weak, about a factor of 4-10 smaller than the calibration difference effects we are studying. This makes clouds a good target for characterization of calibration difference between different instruments simultaneously observing the same cloud fields.

3.4 Spectral adjustment of the empirical regression. Solar irradiance model

To interpret the slopes of the empirical regression in terms of gain ratios, the numbers in the 1st row of Table 1 must be corrected using the theoretically expected slopes in the 2nd row. Results of this correction are listed in the 3rd row. With this adjustment, MISR-MODIS band gain differences for TOA reflectance become +6.0%, +3.3%, +2.7%, and +0.8% for the Blue, Green, Red and NIR bands, respectively. The only band with a non-zero intercept is the Blue. More analyses are needed to fully understand the anomalous behavior of this band.

MODIS TOA reflectance is a primary L1B product obtained by normalizing the detector's readout with the SD measurement. The L1B radiance is calculated from the reflectance using the in-band irradiance. The MISR primary validated L1B product is absolute radiance, and L1B reflectance is calculated next using the total spectral irradiance. The spectral irradiance is a calculated quantity depending on the spectral solar irradiance model (SIM) selected. Presently, due to the lack of high accuracy exo-atmospheric measurements, the SIM is not standardized. The models used by the MODIS and MISR calibration teams are slightly different (see Figure 1). MODIS uses a combination of *Thuillier et al*. [26] (0.4-0.8 μm), *Neckel and Labs* [27] (0.8-1.1 μm), and *Smith and Gottlieb* [28] (above 1.1 μm), whereas MISR uses the values of solar irradiance published by the World Climate Research Program (WCRP 1986) [29]. The maximal difference for the spectral intervals covered by the band-pass functions is in the blue part of spectrum. Our radiative transfer model also uses a high-resolution (1 cm^{-1}) Kurucz [30] model built-in in MODTRAN4.0.

We calculated spectral irradiance $E_{\Delta\lambda}$ (Eq. 2) using both MODIS and MISR SIMs. The ratio of these values is given in Table 4 for MODIS bands and MIRS spectral channels. Not unexpectedly, the difference in SIMs significantly affects the Blue band whereas in the other bands the effect is small. Thus, the difference in the solar irradiance model can explain from 2.1% to 3.6% of our estimate of the reflectance calibration difference (6.0%) in the blue band. Indeed, since the MISR validation is based on matching the TOA radiance, selection of smaller spectral irradiance implies proportionally larger reflectance factor.

The above values of spectral irradiance were also compared with $E_{\Delta\lambda}$ computed with the high-resolution model of Kurucz. In the Blue-Red bands, it agreed well with results obtained with MISR SIM, and in the Green-NIR bands it agreed with

Sensor/Band	Blue	Green	Red	NIR
MODIS	1.0361	1.0040	0.9984	1.0029
MISR	1.0212	1.0028	1.0010	1.0067

Table 4. Ratio of in-band irradiance calculated with MODIS and MISR solar irradiance models ($E_{\Delta\lambda}^{MODIS\_SIM} / E_{\Delta\lambda}^{MISR\_SIM}$) in MISR and MODIS land channels.

results obtained with MODIS SIM. On the other hand, slope and offset of the theoretically calculated regressions practically do not depend on SIM.

Application of the derived gain adjustment factors led to a factor of 2 better agreement between ASRVN albedos obtained from MODIS and MISR data.

4. CONCLUSIONS

This work started with the observation of the systematic biases between the surface albedo and BRF retrieved by ASRVN from MODIS and MISR data near AERONET sites, which is most likely explained by calibration inconsistencies between the two sensors. Using TOA regression method over clouds with spectral adjustment, the following cross-sensor calibration biases were found: 6.0% in the Blue (of which about half is due to the difference in the solar irradiance model), 3.3% in the Green, 2.7% in the Red, and 0.8% in the NIR bands. These discrepancies are generally within the calibration uncertainties of the two instruments, 2-4% for MISR absolute radiance, and 2% for MODIS reflectance. However, they may lead to observable systematic differences in the geophysical parameters affecting multi-instrument data analysis and data fusion approaches. For example, the derived band gain difference is spectrally-dependent, increasing from NIR to Blue band. This can be important e.g. for the aerosol particle size and

mixture composition retrievals as it affects spectral slope of aerosol optical thickness (e.g. [31]). Furthermore, the systematic difference in surface albedo of 0.01-0.03 in the visible part of spectrum may bias retrievals of vegetation parameters, important for global carbon analysis.

Acknowledgements: This work was supported by the NASA EOS Science (Dr. D. Wickland) and NPP (Dr. J. Gleason) grants. The first author thanks Dr. S. Platnick (NASA GSFC) for suggestions on regression analysis over clouds. The work of R. Kahn is supported in part by NASA's Climate and Radiation Research and Analysis Program, under H. Maring, and in part by the EOS-MISR instrument project; it is performed at the Jet Propulsion Laboratory, California Institute of Technology, under contract with NASA. The work of A. Ignatov was funded under the NASA EOS/CERES Project (NASA contract L-90987C). The views, opinions, and findings contained in this report are those of the authors and should not be construed as an official NASA, NOAA or U.S. Government position, policy, or decision.

REFERENCES

1. NASA, 1999. M. King, & R. Greenstone (Eds.), *EOS reference handbook: a guide to Earth Science Enterprise and the Earth Observation System* (p. 355). Greenbelt, MD: EOS Project Science Office, NASA/Goddard Space Flight Center.
2. Xiong X., N. Che, and W.L. Barnes, "Five-year of Terra MODIS On-orbit Spectral Characterization", *Proceedings of SPIE – Earth Observing Systems* X, **5882**, 58820R, doi:10.1117/12.614090, 2005b.
3. Bruegge, Carol J., Wedad A. Abdou, David J. Diner, Barbara J. Gaitley, Mark C. Helmlinger, Ralph A. Kahn, and John V. Martonchik (2004). Validating the MISR radiometric scale for the ocean aerosol science communities. Proceedings of the The International Workshop on Radiometric and Geometric Calibration, December 2-5, 2003, Gulfport, Mississippi. A. A. Balkema Publishers, Rotterdam, Netherlands.
4. Thome, K, Biggar S. Choi H. J., Vicarious calibration of TERRA ASTER, MISR, and MODIS, Conference on Earth Observing Systems IX, Aug. 2-6, 2004. Earth Observing Systems IX: 290-299, 2004.
5. Holben, B. N., T. F. Eck, I. Slutsker, D. Tanré, J. P. Buis, A. Setzer, E. Vermote, J. A. Reagan, Y. J. Kaufman, T. Nakajima, F. Lavenu, I. Jankowiak, A. Smirnov, AERONET-A Federated Instrument Network and Data Archive for Aerosol Characterization, *Rem. Sens. Environ.*, **66,** 1-16, 1998.
6. Guenther B., X. Xiong, V.V. Salomonson, W.L. Barnes, and James Young, "On-Orbit performance of the Earth Observing System Moderate Resolution Imaging Spectroradiometer; first year of data", *Remote Sensing of the Environment*, **83**, 16-30, 2002.
7. Xiong X., J. Sun, J. Esposito, B. Guenther, and W.L. Barnes, "MODIS Reflective Solar Bands Calibration Algorithm and On-orbit Performance", *Proceedings of SPIE – Optical Remote Sensing of the Atmosphere and Clouds* III, **4891**, 95-104, 2003a.
8. Xiong X, K. Chiang, B. Guenther, and W.L. Barnes, "MODIS Thermal Emissive Bands Calibration Algorithm and On-orbit Performance," *Proceedings of SPIE – Optical Remote Sensing of the Atmosphere and Clouds* III, **4891**, 392-401, 2003b.
9. Xiong X., K. Chiang, J. Esposito, B. Gunther, and W.L. Barnes, "MODIS on-orbit calibration and characterization", *Metrologia*, **40**, 89-92, 2003c.
10. Xiong X., J. Sun, J. Esposito, X. Liu, W.L. Barnes, and B. Guenther, "On-orbit Characterization of a Solar Diffuser's Bi-directional Reflectance Factor Using Spacecraft Maneuvers", *Proceedings of SPIE – Earth Observing Systems* VIII, **5151**, 375-383, 2003d.
11. Xiong X., N. Che, and W. Barnes, "Terra MODIS On-Orbit Spatial Characterization and Performance", *IEEE Trans. Geosci. Remote Sensing*, **43**, 355-365, 2005a.
12. Xiong X., H. Erives, S. Xiong, X. Xie, J. Esposite, J. Sun, and W.L. Barnes, "Performance of Terra MODIS Solar Diffuser and Solar Diffuser Stability Monitor", *Proceedings of SPIE – Earth Observing Systems* X, **5882**, 58820S, doi:10.1117/12.615334, 2005c.
13. Bruegge, Carol J., Nadine L. Chrien, Robert R. Ando, David J. Diner, Mark C. Helmlinger, Wedad A. Abdou , Kurtis Thome, "Early validation of Multi-angle Imaging SpectroRadiometer (MISR) radiometric scale", *IEEE Trans. Geosci. Remote Sens*., **40** (7), 1500-1511, 2002.
14. Chrien, Nadine, L, Carol J. Bruegge, and Robert R. Ando, "Multi-angle Imaging SpectroRadiometer (MISR) On-Board Calibrator (OBC) In-flight Performance Studies", *IEEE Trans. Geosci. Remote Sensing* **40** (7), 1493-1499, 2002.

15. Diner, D. J., R. A. Kahn, C. J. Bruegge, J. V. Martonchik, W. A. Abdou, B. J. Gaitley, M. C. Helmlinger, O. V. Kalashnikova, and W-H. Li, "Refinements to MISR's radiometric calibration and implications for establishing a climate-quality aerosol observing system", *Proc. SPIE* **5652**, 57-65, 2004.
16. Kahn, R., W-H. Li, J. Martonchik, C. Bruegge, D. Diner, B. Gaitley, W. Abdou, O. Dubovik, B. Holben, S. Smirnov, Z. Jin, and D. Clark, "MISR low-light-level calibration, and implications for aerosol retrieval over dark water", *J. Atmos. Sci*. **62**, 1032-1062, 2005.
17. Vermote, E., and Y. Kaufman, "Absolute calibration of AVHRR visible and near-IR channels using ocean and cloud views", *Int. J. Remote Sensing*, **16**, *13*, 2317-2340, 1995.
18. Doelling, D., L. Nguyen, and P. Minnis, "On the use of deep convective clouds to calibrate AVHRR data", Proc. SPIE, 5542, 281-289, 2004.
19. C. Cox and W. Munk, "Measurements of the roughness of the sea surface from photographs of the Sun's glitter," *J. Opt. Society Am.* **44**, 838-850, 1954.
20. Bruegge, C. J., N. L. Chrien, D. J. Diner, Level 1 in-flight radiometric calibration and characterization algorithm theoretical basis, Jet Propulsion Laboratory, JPL D-13398, Rev. A., 128 p, December 1999.
21. Lyapustin, A., "Radiative transfer code SHARM for atmospheric and terrestrial applications", *Appl. Optics*, **44**, 7764-7772, 2005.
22. Lyapustin, A., "Interpolation and Profile Correction (IPC) method for shortwave radiative transfer in spectral intervals of gaseous absorption," *J. Atmos. Sci.* **60**, 865-871, 2003.
23. Rothman L. S., Barbe A., Benner D. C., Brown L. R., Camy-Peyret C., Carleer M. R., Chance K. V., Clerbaux C., Dana V., Devi V. M., Fayt A., Flaud J.-M., Gamache R. R., Goldman A., Jacquemart D., Jucks K. W., Lafferty W. J., Mandin J.-Y., Massie S. T., Nemtchinov V., Newnham D. A., Perrin A., Rinsland C. P., Schroeder J., Smith K. M., Smith M. A. H., Tang K., Toth R. A., Vander Auwera J., Varanasi P., Yoshino K., "The HITRAN Molecular Spectroscopic Database: Edition of 2000 Including Updates through 2001". *J. Quant. Spectrosc. Radiat. Transfer*, **82**, 5-44, 2003.
24. Mlawer, E. J., D. C. Tobin, and S. A. Clough, "A Revised Perspective on the Water Vapor Continuum: The MT_CKD Model", in preparation, 2006.
25. Hale, G. M., and M. R. Querry, "Optical constants of water in the 200-nm to 200 μm wavelength region," *Appl. Optics* **12**, 555-563, 1973.
26. Thuillier G., Herse M., Simon P. C., et al., "The visible solar spectral irradiance from 350 to 850 nm as measured by the SOLSPEC spectrometer during the ATLAS I mission", *Solar Physics* **177** (1-2), 41-61, 1998.
27. Neckel, H., D. Labs, "The solar radiation between 3300 and 12500 A", *Solar Physics* **90**, 205-258, 1984.
28. Smith E. V. P., Gottlieb D. M., "Solar flux and its variations", *Space Science Reviews* **16** (5-6), 771-802, 1974.
29. World Climate Research Program (WCRP) Publication Series No 7, WMO ITD – No: 149: 119-126, October 1986. The data was compiled by Cristoph Wehrli. World Radiation Center (NRC). Davos-Dorf. Switzerland, under WRC Publication, No 615, July 1985.
30. Kurucz, R. L., 1997, The solar irradiance by computation. Available at http://cfaku5.cfa.harvard.edu/ papers/irradiance/.
31. Ignatov, A, "Sensitivity and information content of aerosol retrievals from AVHRR: Radiometric factors", *Appl. Opt*., **41**, *6*, 991-1011.